Aalborg Universitet

AALBORG UNIVERSITY

DENMARK

Results of Caisson Breakwater Tests in Multidirectional Breaking Seas

internal laboratory test reportzs

Kofoed, Jens Peter

Publication date:
1997

Document Version
Publisher's PDF, also known as Version of record

[Link to publication from Aalborg University](#)

Citation for published version (APA):
Kofoed, J. P. (1997). *Results of Caisson Breakwater Tests in Multidirectional Breaking Seas: internal laboratory test reportzs*. Hydraulics & Coastal Engineering Laboratory, Department of Civil Engineering, Aalborg University.

Results of Caisson Breakwater Tests in Multidirectional Breaking Seas

(Internal Laboratory Test Report)

Hydraulics and Coastal Engineering Laboratory
Dept. of Civil Engineering
Aalborg University
Denmark
December 1997

Contents

1   Introduction

In extension of the work done at the Hydraulics and Coastal Engineering Laboratory, Dept. of Civil Engineering, Aalborg University, Denmark, described in Grønbech et al.,1997, laboratory tests has been performed investigating wave loading and overtopping on caisson breakwaters in multidirectional breaking seas.

simultanel --

The effects of wave obliquity and multidirectionality on the wave loads were investigated by measuring the wave induced pressure at 8 points in vertical section at different positions on a 4.0 m wide caisson breakwater model, enabling determination of the horizontal force in one vertical line at the front of the caisson as well as the lateral distribution of the horizontal force. The horizontal force in one section is investigated in terms of the statistical force parameter $F_{1/250}$, while the lateral distribution is investigated in terms of the correlation coefficient ρ between the horizontal force signals at different locations.

The wave overtopping was measured on a 0.3 and 0.1 meter wide section of the caisson breakwater model. The effect of wave obliquity and multidirectionality are investigated in terms of the mean average overtopping discharge $\overline{q}$ as well as the statistical overtopping discharge parameter $q_{1/250}$.

2   Experimental setup

The laboratory tests were carried out in the 3D deep water wave basin at the Hydraulic and Coastal Laboratory, Dept. of Civil Engineering, Denmark. The basin is equipped with wave generators capable of generating irregular multidirectional waves.

Using the experiences from the previously performed tests, the setup shown in Figure 1 and 2 was chosen.

The caisson breakwater model was constructed in plywood and placed on a smooth one layer foundation berm. Since the wave induced uplift pressures at the caisson bottom was not considered in the study, the foundation berm was constructed in concrete. The cross section of the model is seen in Figure 1. The size of the model does not refer to any particular prototype structure, however, a Froude scaling of 1:20 - 1:25 seems appropriate for this type of structures. In order to generate a sea state representing breaking waves in front of the caisson model, a relatively short 1:5 slope was constructed and placed as seen in Figure 1.
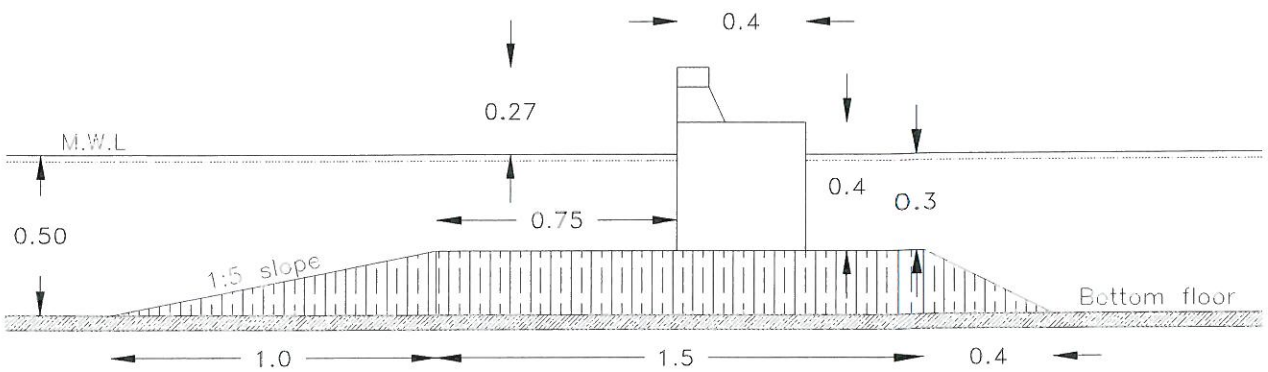

Figure 1: Cross section of caisson model.

Previous investigations have shown that the presence of the slope in front of the structure results in

wave breaking of 6 - 7 % of the irregular waves, using a significant wave height $H_S = 0.18\ m$, see Grønbech et al., 1997, p. 2.

The experimental setup in plan view is shown in Figure 2.
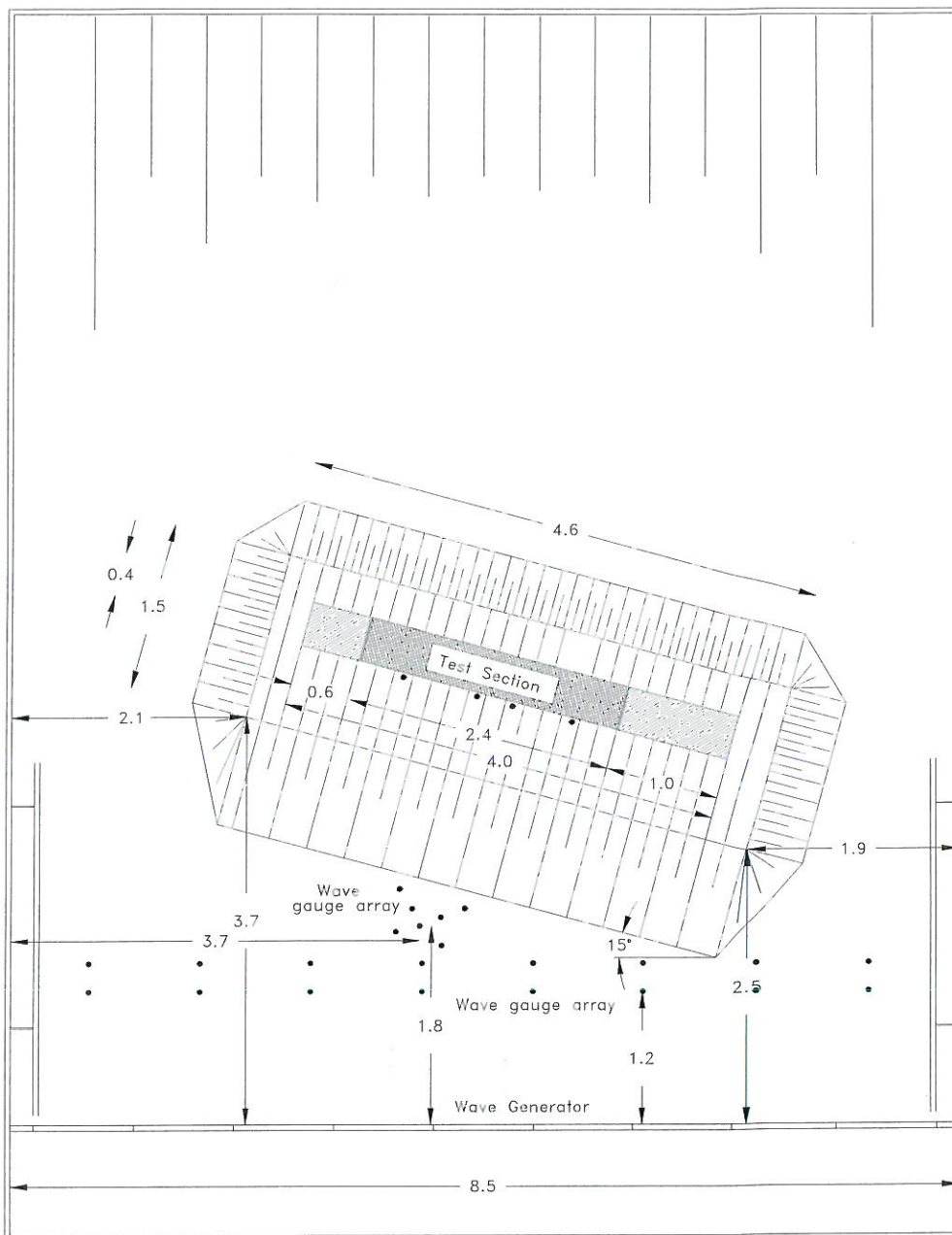
Figure 2: Plan view of the experimental setup.

Due to the wave diffraction processes around the two ends of the breakwater, the sea states in the vicinity of the ends would be disturbed during the tests. Therefore, since the lateral distribution of the horizontal force was to be considered in this study, it was important that the sea state in front of the test section not was influenced by the diffraction at the two ends. On this basis it was chosen to use a 4.0 m wide vertical breakwater, were 2.4 m in the middle was used as the test section. Thus, the width of the structure has been reduced compared to the previous tests, where the structure was 6.0 m. This was done in order to reduce the amount of wave energy reflected by the structure, and because the structure has been turned so the angle between the the wave generators and the front of the structure now is 15° compared to 30° as in the previous tests. By turning the

4

structure generation of oblique multidirectional waves with higher quality was enabled, as it was experienced in the previous tests that generating waves with a mean direction deviating more than 15° from perpendicular to the wave generator, entailed unwanted diffraction along the sides of the basin. Thus, this limits the range of the angle of wave attack θ on the structure in which high quality waves can be achieved to 0° - 30°. Accepting the same amount of diffraction along the basin sides as in the previous tests, values of θ up to 45° can be achieved.

Along the side walls of the basin, vertical steel absorbers were placed to damp any cross modal activity occurring during the tests. At the rear end of the basin a spending beach constructed of gravel material was placed in order to absorb the wave energy that passed the structure.

As the structure has a significant width compared to the width of the basin and it is a highly reflective structure, it was expected that a large amount of the energy in the generated waves would be reflected and re-reflected, and thus unable control of the generated wave field, if steps was not taken to prevent this. Therefore, an on-line active absorption system was used. The system operates by digital filtering of the surfaces elevations measured in 16 individual positions organised in 2 parallel rows in front of the wave generator, see Figure 2. The wave absorption system is in its complete form outlined in Hald and Frigaard, 1997.

2.1   Wave gauge setup

In addition to the wave gauges used in the active wave absorption system, an array of 7 wave gauges are used to determine the 3D wave field parameters of the incident waves at deep water, i.e. in front of the berm, see Figure 2. This is done by using the Bayesian Directional spectrum estimation Method (BDM). This method and the PASCAL program used is described in Hydraulics and Coastal Engineering Laboratory, 1997.

For estimation of the wave field parameters at shallow water on the front of the structure, each position of the wave pressure gauges, measuring the horizontal force, is equipped with a wave gauge. If full reflection by the structure is assumed, an estimate of the wave height at the front of the structure can be achieved.

For both the wave gauges at deep and shallow water a sample frequency of 10 Hz was used.

2.2   Pressure gauge setup

The 2.4 m of the structure within which measurements where performed, was designed so it was possible to easily move the array of the 8 pressure gauges setup on the vertical line from which the horizontal force was calculated. As the total number of pressure gauges was limited by the number of the channels available on the A/D-card used to sample the pressures, it was decided to equip 4 sections with pressure gauges. Thus, measurements of forces could be performed at 4 positions simultaneously. The layout of each section with pressure gauges are shown in Figure 3.

As the water depth at the berm is 0.3 m and the height of the structure over the mean water level (MWL) R_c is 0.27 m, it can be seen from Figure 3 that on pressure gauge is placed in MWL (gauge 4), 3 above (gauge 1 - 3) and 4 under (gauge 5 - 8). It is expected that this gives a fair resolution of the pressure profile, so that the horizontal force can found by integration of the pressures sampled by the pressure gauges.

In order to ensure that even very short impact forces from the breaking waves are recorded, the pressures was sampled using a frequency of 800 Hz.
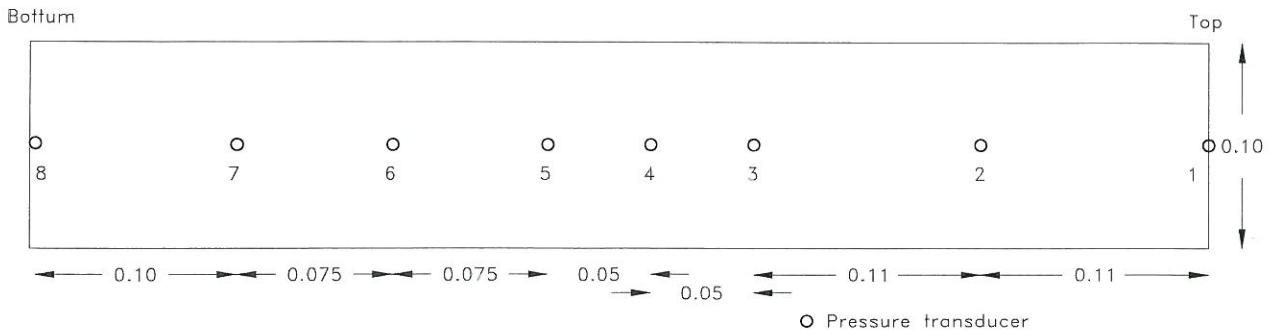
Figure 3: Layout of a pressure gauge section (turned 90° clockwise).

On the structure 10 positions were prepared for the pressure gauge sections, see Figure 4.

This enables the investigation of the correlation coefficient ρ for a large variety of distances x between the measuring positions. Thus, using 4 measuring sections up to 6 corresponding values of x and ρ can be achieved. Then by repeatedly using the same generated wave time series, but different positions of the measuring sections, a large number of corresponding values of x and ρ can be found, but in these tests the number of tests performed with the same generated wave time series was limited to 2. The configuration of the measuring sections were EFGI and ACGJ, respectively. Thus, this results in 9 different values of x, namely $x = 0.1, 0.3, 0.6, 0.8, 0.9, 1.5, 1.8, 2.4\ m$. Of these the value 0.6 m is occurring twice and 0.9 m 3 times. This is advantageous as it can be used as an indication of the deviation of the results and a connection between the 2 performed tests.
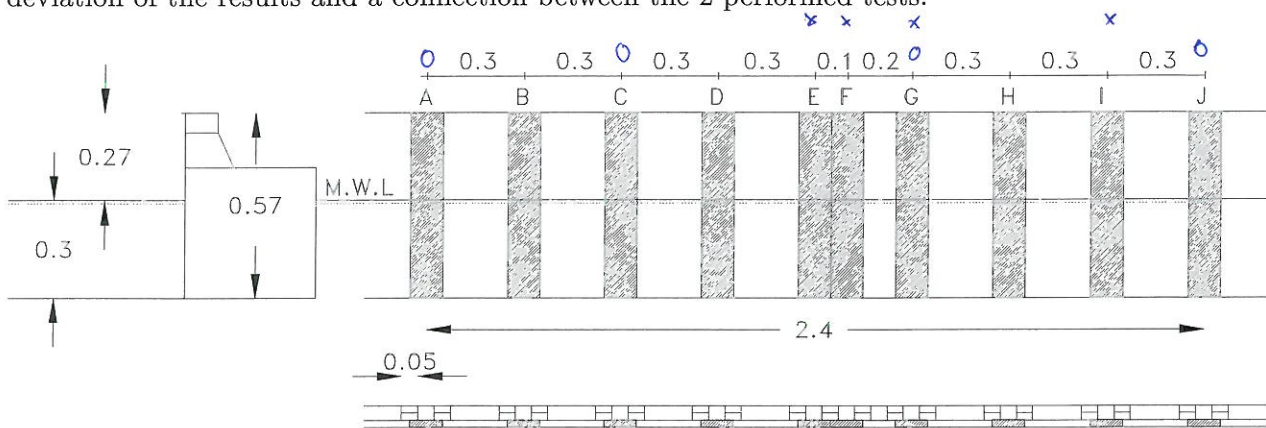

Figure 4: Layout of the front of the structure (hatch indicates the 10 positions where pressure gauge sections can be placed).

2.3 Wave overtopping measuring setup

The amount of overtopped water is measured by a device shown in Figure 5. The lensing pipeline is connected to a pump which is controlled by the surface elevation in the collector, and empty the collector when a certain level is reached by pumping the water back into the wave basin. Furthermore, a water meter is connected to the pump from which the amount of pumped water can be read. The structure is actually equipped with two overtopping collectors with a width of 0.3 and 0.1 m, respectively. As each test is performed twice, cf. above, only one of the devices are active at same time. By registration of the surface elevation level and the water meter reading at the beginning and the end of a test, the mean average overtopping discharge $\bar{q}$ can be found. Furthermore, the surface

elevation level is sampled by the wave gauge indicated in Figure 5 with sample frequency of 10 Hz. By analysis of this signal the $q_{1/250}$ can be determined.
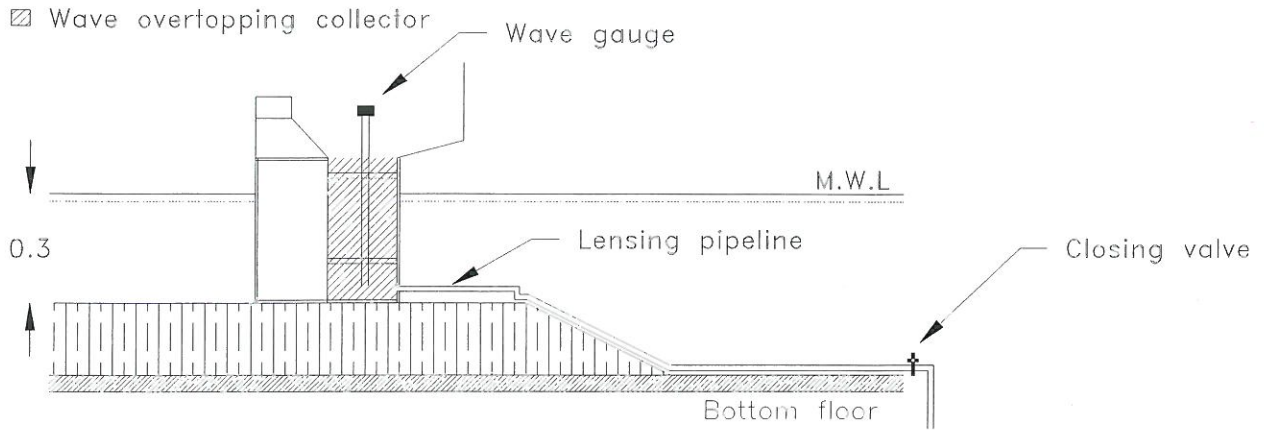

Figure 5: Wave overtopping measuring device.

3   Test conditions

As the main objective of the performed tests was to assess the effect of wave obliquity and multi-directionality the changes on test conditions were the incident mean direction of the waves and the directional spreading of the waves, i.e. the energy distribution around the mean direction of the waves. The mean direction or the incident angle of wave attack was varied from 0 (head on waves) to 45° for some of the tests. A cosine squared $cos^{2s}(\frac{\theta}{2}))$ directional spreading function with s-parameters corresponding to standard deviations of 18° and 25°.

The incident target wave height was fixed at 0.18 m for the breaking waves. A JONSWAP wave spectrum with a peak enhancement factor of 3.3 and a peak period T_P of 1.2 s was applied in all the tests, giving a steepness at 0.08 for breaking waves. To obtain an adequately statistically validity of the test results, test series of 30 minutes were performed. This corresponds to 1950 waves in average, assuming that the average period is $\frac{T_P}{1.3}$ as given in NtH.

In Table 1 the parameters for which tests have been performed is shown.

Wave spectrum	JONSWAP, $\gamma = 3.3$
Significant wave height, H_S	0.18 m
Peak period, T_P	1.2 s
Crest freeboard, R_c	0.27 m
Waterdepth, deep water, h_d	0.5 m
Waterdepth, shallow water, h_s	0.3 m
Angle of wave attack, θ	0°, 15°, 30°, (45°)
Type of directional spreading	Cosine squared, $\sigma = 18°$, $\sigma = 25°$

Table 1: Target wave parameters used in the performed tests.

The wave fields was generated using the wave generation system PROFWACO (see XX) to generate the time series. These time series were then used as input to the active absorbtion system, which controlled the wave generator.

7

In order to achieve the target wave parameters within an acceptable margin some preliminary tests were performed. Hereby the appropriate wave generation input parameters were found.

4 Wave force analysis

In the analysis of the wave forces first the pressures measured in one section is converted into the horizontal force signal by linear integration. In Figure 6 an example of a 10 s time series from a test series with head on waves ($\sigma = 18°$.) is shown.
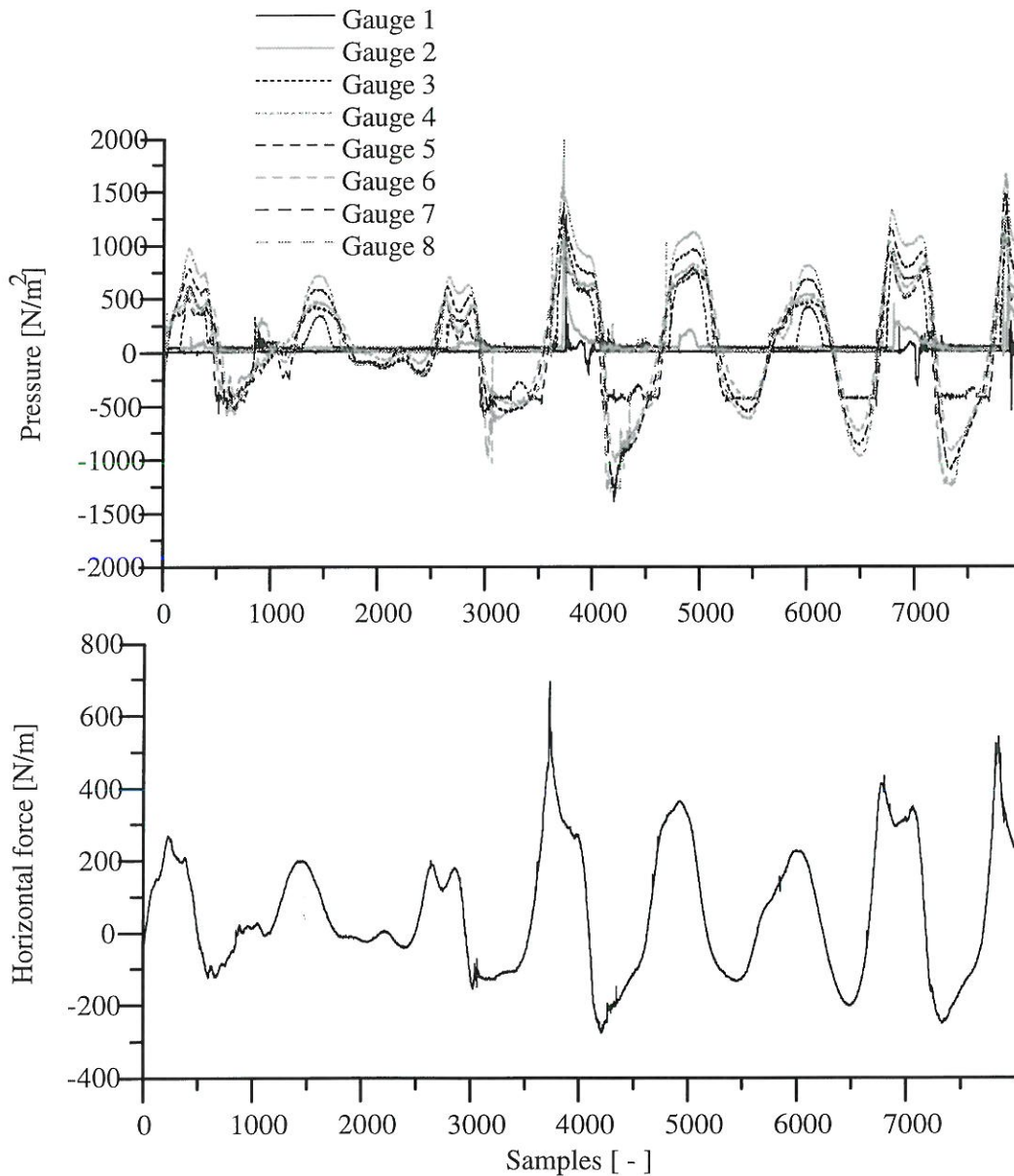

Figure 6: 10 s of sampled pressures and corresponding force from one section.

In Figure 7 the pressure distribution corresponding to the 6.000^{th} set of sampled pressures in Figure 6 is shown.

By calculating the force time series for each 4 sections in each performed tests, the basis for the further analysis was established, and the probability distribution of the horizontal forces were then found for each force time series. In the finding of this probability distribution only the maximum
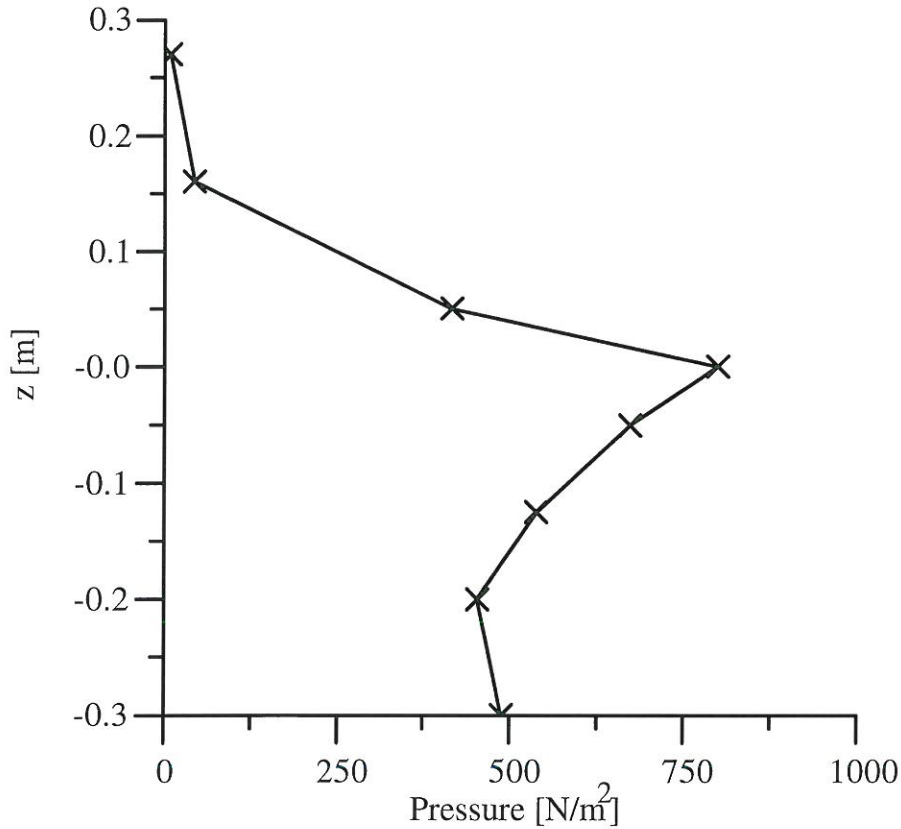
Figure 7: The pressure distribution corresponding to the 6.000^{th} sample from Figure 6.

peaks within a time window of 0.75 s was considered. From the probability distribution the $F_{1/250}$ was calculated as the average of the 8 largest maximum peaks, since it was assumed that a time series consists of approximately 1.950 waves (cf. earlier section).

4.1 Comparison between measured and predicted wave forces

The evaluation of the measured forces are done by comparison with a predicted horizontal wave force calculated by use of Goda's method as described in Allsop et al., 1996. The Goda force is calculated under the assumption that the caisson is placed directly on the sea bed (i.e. no berm) with a water depth of 0.3 m. This is due to the fact that the berm is introduced in the tests not in order to model a berm, but to achieve wave breaking in front of the structure. When calculating the Goda force both the deep and shallow water H_S have been used, resulting in two different Goda forces for each test, see Figure 8 and 9 respectively. This also means that for the deep water results the same H_S has been used for all four sections in each test, while for the shallow water results the H_S found at each cross section is used. This means that the any effects of diffraction around the ends of the structure that might occur, causing different wave heights at different locations on the structure, is extracted from the shallow water results. In the figures the results of each test are shown as points. Furthermore, the average of the results for each direction are marked as a line. As mentioned earlier, two tests were performed generating the same wave field but measuring the forces at different locations on the structure. Therefore, two results are shown for each cross section, direction and directional spreading.

From the figures it can be seen that no significant difference between the results based on deep and shallow water wave heights were found. This indicates that the effects of wave breaking (decreasing the wave heigt) and shoaling (increasing the wave height) level each other out.
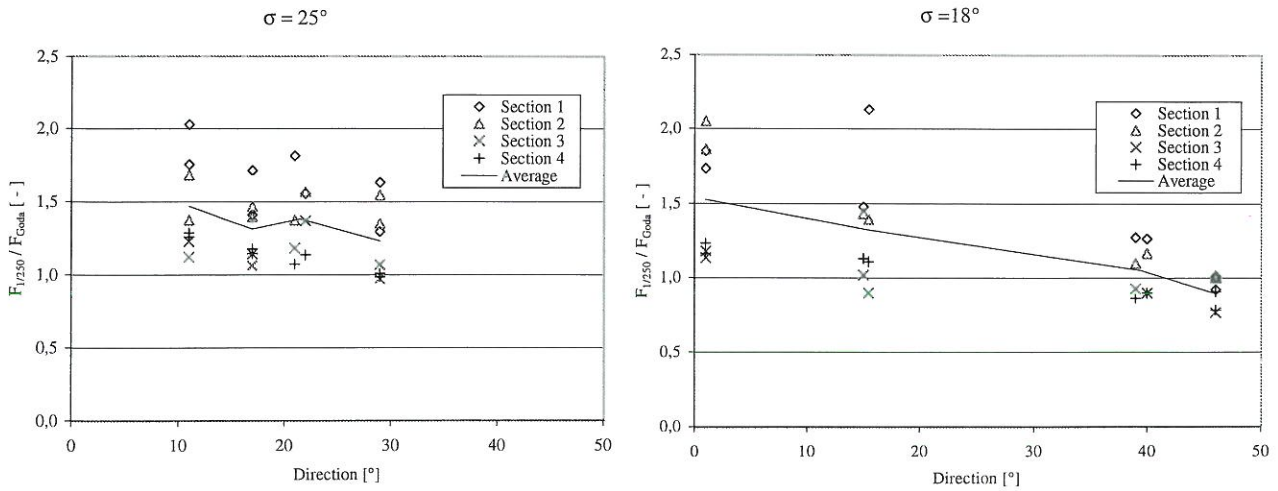
9

Figure 8: Measured forces normalised with Goda force on deep water.

Considering the mean value it is seen that the ratio between the measured and calculated force is decreasing for increasing angle of wave attack. This indicates that the Goda method does not sufficiently take the effect of the obliqueness of the waves into account. Furthermore, it is seen that the ratio for small angles of wave attack is around 1.5, which indicates that the Goda method underestimate the horizontal wave force in this range.
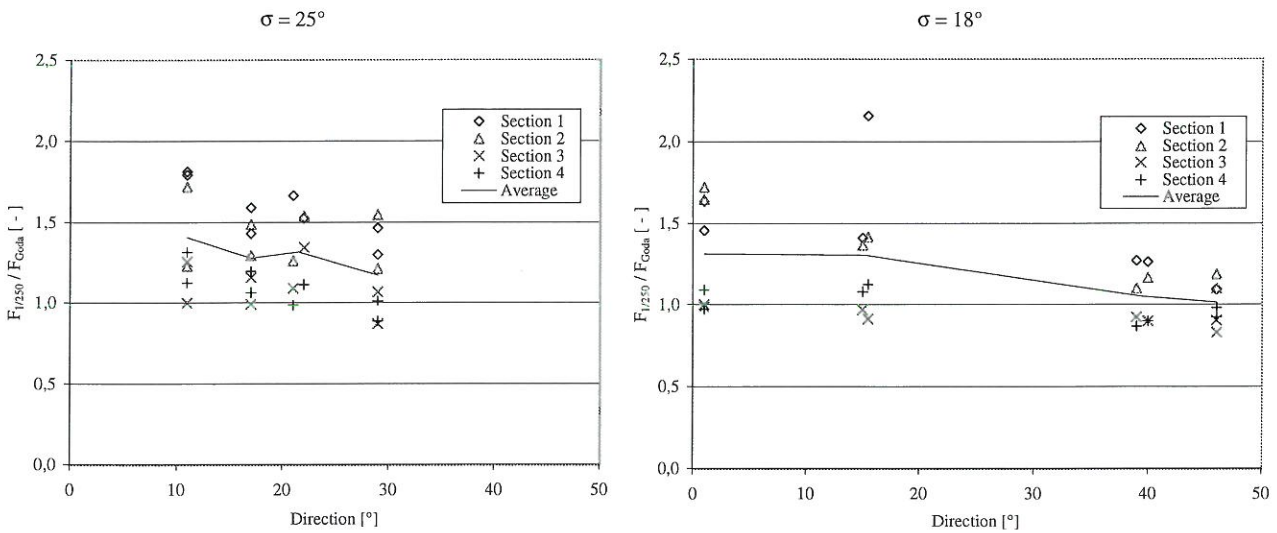

Figure 9: Measured forces normalised with Goda force on shallow water.

Regarding the points in the figures a relatively large amount of scatter around the average for each angle of wave attack and directional spreading is observed. But by taking a closer look, it can be seen that the results from section 1 and 2 for almost all tests are below the average, while the results from section 3 and 4 are above. Since each section is used to measured at different positions on the structure, and there are no significant difference between the deep and shallow water results, this cannot be a "true" effect but is most likely an effect of the used measuring equipment. In the setup of the pressure measuring device, two different amplifiers were used, one for the first 16 channels (corresponding to section 3 and 4) and another one for the last 16 channels (corresponding to section 3 and 4). Thus, it is possible that consequent difference in the results in section 1 and 2 and section

10

3 and 4 is an effect of different capabilities of the used amplifiers. Actually, the amplifier used for section 3 and 4 was not able to process as short peaks as the amplifier used for section 1 and 2, due to differences in the analog circuits in the amplifiers, and therefore some of the very short but large impacts might have been sampled in section 1 and 2, but not in section 3 and 4. This means that the results shown for section 1 and 2 probably are more correct that the results found in section 3 and 4. However, if only the results from section 1 and 2 are regarded, basicly the same conclusion as mentioned above can be made, except that the trends are even more significant for these two sections.

4.2 Determination of correlation coefficient function ρ

As earlier mentioned another main purpose of the tests was to investigate the lateral distribution of the horizontal wave force. This has been done by calculation of the correlation coefficients between the wave force signals at different positions on the structure. The correlation coefficient ρ between the force signals F_1 and F_2 has been calculated as

$$\rho_{F_1,F_2} = \frac{1}{N} \sum_{i=1}^{N} \frac{(F_{1,i} - \mu_{F_1})(F_{2,i} - \mu_{F_2})}{\sigma_{F_1} \sigma_{F_2}} \tag{1}$$

where

F_i is a sample in the force time series.

N number of samples in the time series.

μ is the mean value of the time series.

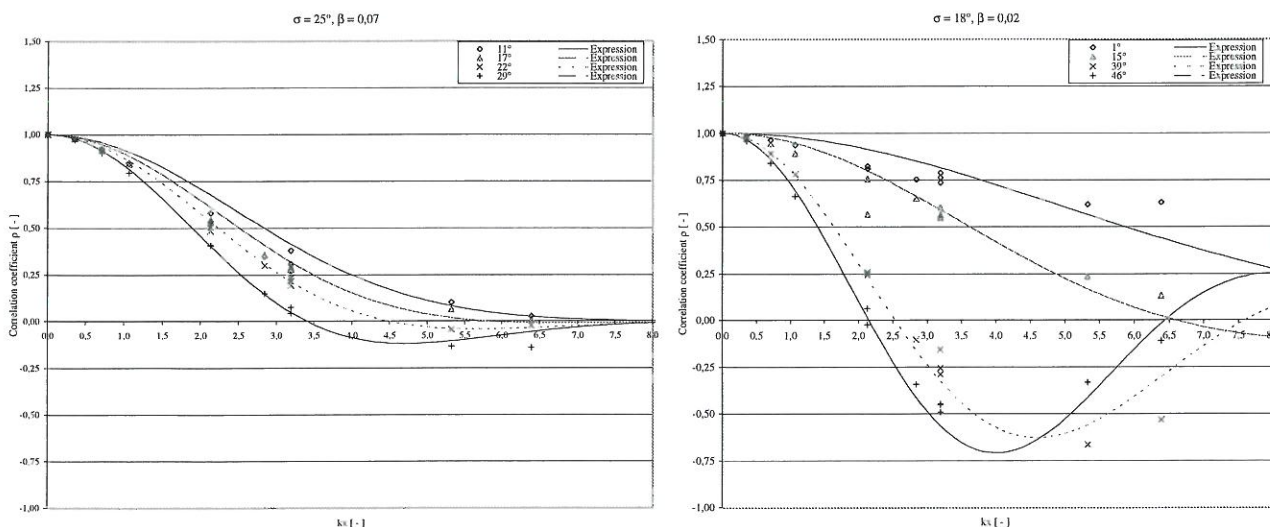σ is the spreading of the time series.

Figure 10: Cross correlation functions for the horizontal wave forces as a function of the wave number times the distance.

The correlation coefficient ρ has been determined for 9 different lateral distances between the cross sections where the force time series were sampled by analysis of the two tests performed for each angle of wave attack and directional spreading. These correlation coefficients are shown as point in

11

Figure 10 where the wave number corresponding to the peak period k times the distance between the cross sections x is used as abcisse.

By performing a regression analysis of the correlation coefficient values ρ, an expression for prediction of ρ as function of kx has been found:

$$\rho(kx) = cos(\alpha kx)e^{-\beta(kx)^2} \tag{2}$$

By investigation of the expression in (2) it is seen that the β value can be interpreted as a parameter governed by the directional spreading in the wave field. The β-value act as a "damping"-coefficient which entails that a larger β-value results in a smaller correlation coefficient for a given distance. This means that more directional spreading was expected to entail larger β-values, and that the β-values was expected only to be dependent of the directional spreading. Furthermore, the α-value was expected to be governed by the angle of wave attack θ, as α is counter proportional to the "wave length" and thus larger θ was expected to result in larger α-values.

The regression analysis showed that it would be fair to set the $\beta = 0.02$ and 0.07 for $\sigma = 18°$ and 25°, respectively. Furthermore, a linear connection between the angle of wave attack θ and the α coefficient was found, as shown in Figure 11.
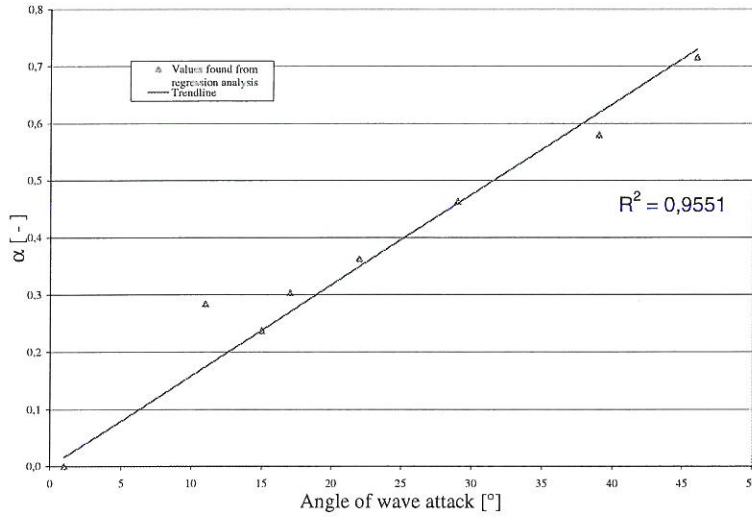

Figure 11: α coefficients fitted to (2) as a function of angle of wave attack θ, and the trendline giving the linear connection between α and θ.

This linear connection was found using both the values from tests with $\sigma = 18°$ and 25°, i.e. the α coefficient is not dependent on the directional spreading in the wave field. Thus, the α coefficient can be found from

$$\alpha = 0.0159\,\theta \tag{3}$$

On this background expression given in (2) can be rewritten as

$$\rho(kx) = cos(0.0159\,\theta kx)e^{-\beta(kx)^2} \tag{4}$$

where

θ is given in degrees, $0°$ head on.

$\beta = 0.02$ for $\sigma = 18°$.

$\beta = 0.07$ for $\sigma = 25°$.

Using (4) the lines in Figure 10 were calculated. In order to give a better impression of how well the expression fits the data, a plot showing the cross correlation coefficients for the measured data $\rho_{measured}$ against values calculated by use of the expression $\rho_{expression}$ is presented in Figure 12.
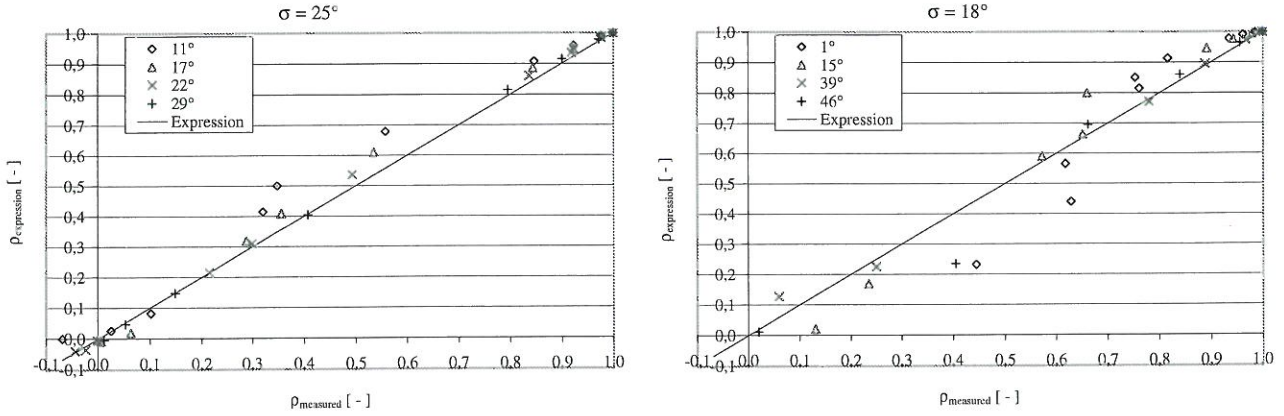

Figure 12: Cross correlation coefficients for the measured data $\rho_{measured}$ plotted against corresponding values calculated by use of the expression $\rho_{expression}$.

Furthermore, the R^2-values for $\rho_{measured}$ against $\rho_{expression}$ have been calculated, see Table 2.

$\sigma = 25°$	
$\theta = 11°$	$R^2 = 0.981$
$\theta = 17°$	$R^2 = 0.994$
$\theta = 22°$	$R^2 = 0.999$
$\theta = 29°$	$R^2 = 0.997$
$\sigma = 25°$	
$\theta = 1°$	$R^2 = 0.913$
$\theta = 15°$	$R^2 = 0.967$
$\theta = 39°$	$R^2 = 0.981$
$\theta = 46°$	$R^2 = 0.986$

Table 2: R^2-values for $\rho_{measured}$ against $\rho_{expression}$.

From Figure 12 and Table 2 it can be seen that the expression given in (4) in general agrees well with the experimental data, allthough some scatter is observed. The largest deviations are observed for the smallest wave attack angles.

5 Wave overtopping analysis

In the analysis of the amount of wave overtopping, at first only the mean average overtopping discharge $\overline{q}$ per meter structure length is considered. Afterwards, the effect of the width of the measuring device

used to measure the amount of wave overtopping is investigated in terms of the statistical overtopping discharge parameter $Q_{1/250}$.

5.1 Comparison between predicted and measured overtopping discharge

From $\overline{q}$ the non dimensional mean overtopping disharge Q is defined as:

$$Q = \frac{\overline{q}}{\sqrt{gH_S^2}} \tag{5}$$

where

g is the gravity acceleration.

H_S is the significant wave height.

The basic assumption, confirmed by many researchers, is that the main parameters influencing the wave overtopping performance, i.e. the significant wave height H_S, the crest height R_C and the non dimensional mean overtopping discharge Q given in (5) are related through the exponential function

$$Q = a\, e^{-\frac{b}{\gamma}\frac{R_C}{H_S}} \tag{6}$$

where

a and b are fitting coefficients.

γ is a reduction factor, taking wave obliquity and multidirectionality into account.

Based on more than 80 hydraulic model tests performed in the Directional Wave Basin at Delft Hydraulics, Franco et al., 1995 suggested the use of $a = 0.082$ and $b = 3.0$ for plain vertical structures exposed to head on waves. Franco et al., 1995 suggested, through a best fit regression analysis, the following relation between the γ and the angle of wave attack θ:

$\gamma = 0.83$ for $0° \leq \theta \leq 20°$
$\gamma = 0.83\, cos(20° - \theta)$ for $\theta \geq 20°$

By calculating the measured non dimensional mean overtopping disharge Q_m on the basis of the $\overline{q}$ found in the laboratory tests using (5), and the predicted non dimensional mean overtopping disharge Q_p based on (6), the $\frac{Q_m}{Q_p}$-ratio was found for each performed test. The results are shown in Figure 13 and 14.

In these figures both the results from the tests where the overtopping device with a width of 0.1 m and 0.3 m are shown. In general the results show that the prediction formula underestimate the amount of overtopping, all though a considerable amount of scatter also is observed. This indicates that the a and b coefficients used does not apply very well for the performed tests.

Considering the graph based on the deep water H_S it is seen that the results found by use of the two different widths of the overtopping measuring device agrees better than for the results based on
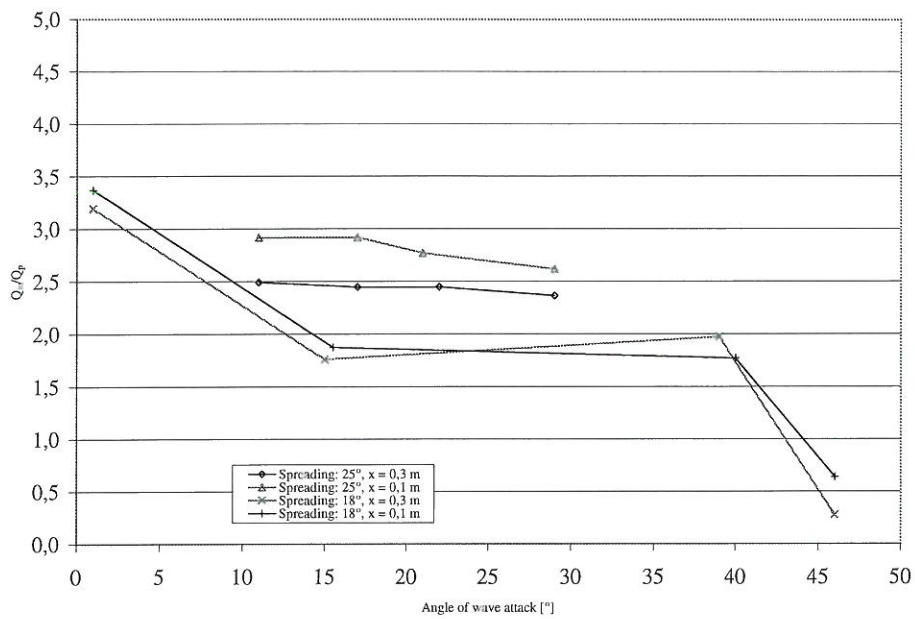
Figure 13: Measured non dimensional overtopping discharge normalised with the corresponding predicted, using (5) and (6) on deep water.
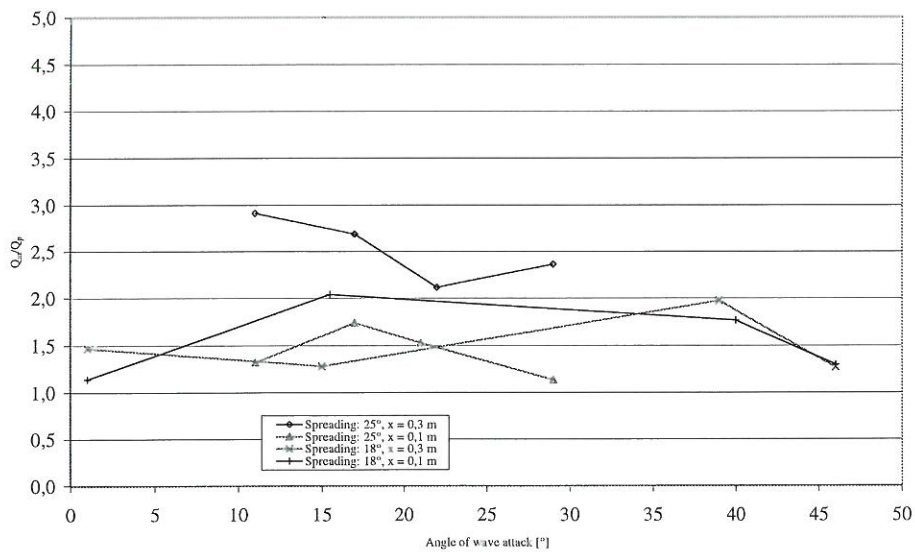

Figure 14: Measured non dimensional overtopping discharge normalised with the corresponding predicted, using (5) and (6) on shallow water.

the shallow water H_S. Furthermore, it is seen that the difference between the results found with the different widths of the overtopping measuring device seems to be increase for increasing directional spreading.

From the results based on the deep water H_S it seems like the reduction factor γ applies well for the tests with $\sigma = 25°$, as the lines are almost constant, while the results for the tests with $\sigma = 18°$ indicates that the used γ-values is incorrect.

5.2 Investigation of the effect of the width of the overtopping measuring device

Using the laboratory tests with different widths of the overtopping measuring device an investigation of this widths influence on the statistical overtopping discharge parameter $q_{1/250}$. It is considered fair to assume that the mean average overtopping discharge $\bar{q}$ per meter structure length is unaffected by change in the width of the overtopping measuring device over long time. But regarding the each overtopping event it is expected that the overtopping discharge per meter structure corresponding to an overtopping event occuring seldom, will become larger as the width of the overtopping measuring device is decreased.
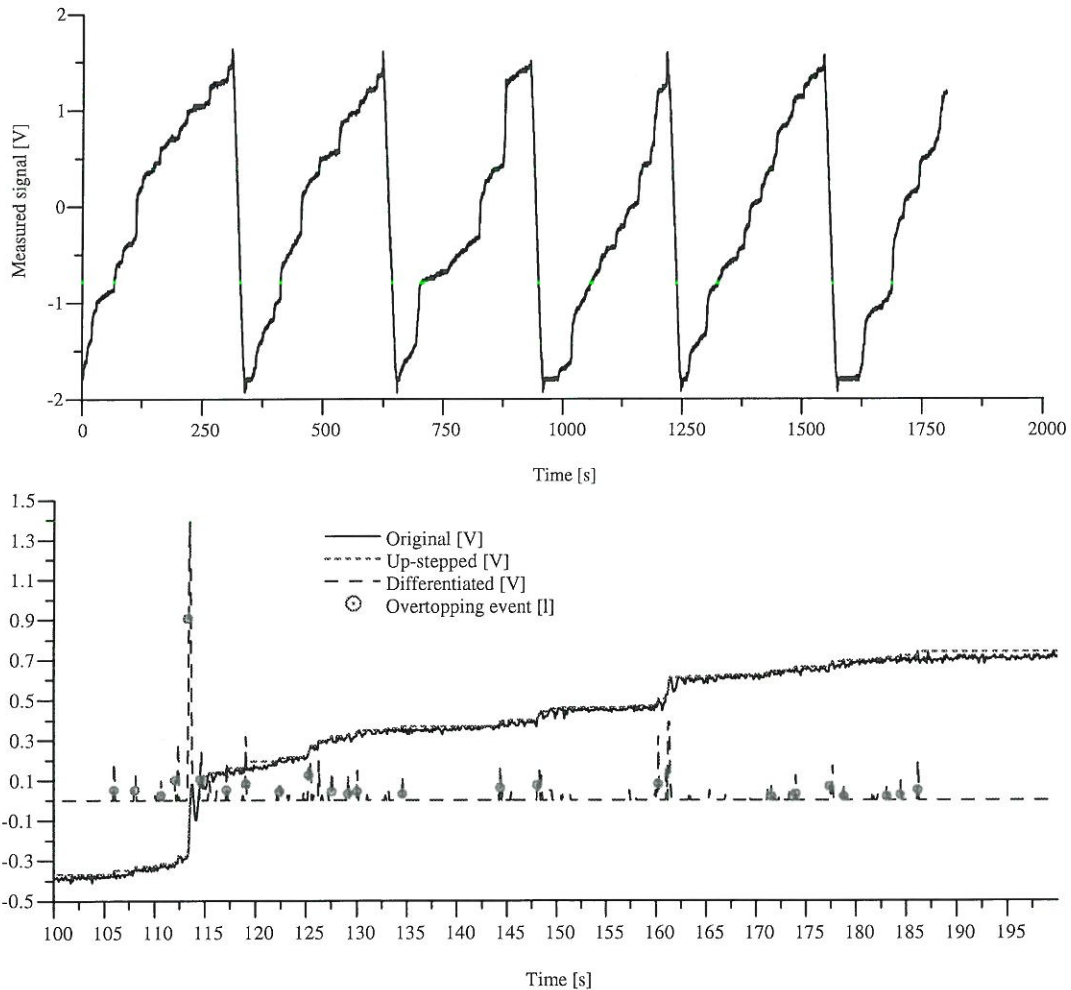

Figure 15: Top: Original signal from gauge in overtopping tank during a test. Bottum: A part of the signal above. The original signal is the solid line, the dotted line is the up-stepped signal, the dashed line is the up-stepped signal differentiated and each circle marks an identified overtopping event and the corresponding overtopping discharge.

16

This is investigated by analyzing the recorded time series of the elevations in the overtopping tank, and hereby identifying the largest overtopping events and the corresponding discharge. From these largest overtopping disharges the statistical overtopping discharge parameter $q_{1/250}$ is defined as the mean value of the 8 largest overtopping disharges found in the time series analysis, as this approximately corresponds to $\frac{1}{250}$ of the number of waves in a time series.

In Figure 15 (top) an example of a signal recorded by the gauge placed in the overtopping tank during a test is shown. In order to determine each overtopping event this signal has been analyzed. At first an up-stepped version of the original signal is found by not allowing the signal to decrease except when the overtopping tank is emptied, see Figure 15 (bottum). This way the high frequency waves in the overtopping tank is filtered out and a more smooth signal is obtained. By differentiating this signal the overtopping events can be identified, as differentiated signal is different from 0 where the water level in the overtopping tank is increased. Though, since it is only the overtopping events resulting in the largest amount of overtopping that is interesting, a threshold is selected for the differentiated signal, which must be exceeded to identify an overtopping event. Furthermore, if the differentiated signal is exceeding the threshold, but there was found another overtopping event within the last 8 timesteps (corresponding to 0.8 s), this exceedens is not regarded as an overtopping event. Thus, it is secured that one large event is not split into more smaller events.

After identifying an overtopping event the corresponding disharge is found by substracting the value of the up-stepped signal corresponding to 3 time steps (corresponding to 0.3 s) after the overtopping event from the the value of the up-stepped signal corresponding to 3 time steps before the overtopping event. This differens is then multiplied by a calibration constant converting it into a overtopping discharge. Thus, it is assumed that there is no waves resulting in large overtopping with a period of 0.6 s corresponding to half of the peak period.

By applying this analysis to all of the sampled time series from the performed tests, and to the corresonding time series from the tests presented in Grønbech et al., 1997, three values of $q_{1/250}$ have been found for each set of angles of wave attack and directional spreading. The three values for each set corresponds to three different widths of the used overtopping measuring device, $x = 0.1$, 0.3 and $1.0m$ respectively. In Figure 16 the results of these analysis are shown in terms of the ratio $q_{1/250}$ normalized with $\bar{q}$.
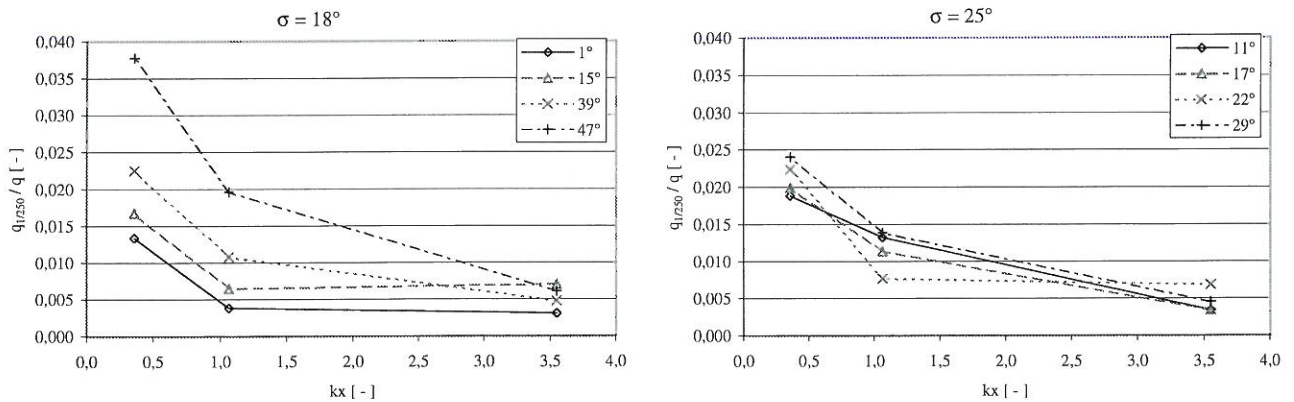

Figure 16: The the statistical overtopping discharge parameter $q_{1/250}$ normalized with the mean average overtopping discharge $\bar{q}$.

From Figure 16 it is seen that in general the ratio is decreased for increasing width of the overtopping measuring device x as expected. This tendency is more pronounced for the time series with a directional spreading $\sigma = 18°$ than for $\sigma = 25°$. Furthermore, it is seen that the ratio is increased as the angle of attack is increased.

17

6 Conclusion

Yet to come!!!

7 Acknowledgements

8 References

Grønbech J., Kofoed J. P., Hald T., Frigaard P. and Burchart H. F. (1997). *Hydraulic Response of Caisson Breakwaters in Multidirectional Breaking and Non-breaking Waves.* To be published in evaluation report on the frame work programme *Dynamics of Structures* of the *Danish Technical Research Council* in April 1998.

Hald T. and Frigaard P. (1997). *Alternative Method for Active Wave Absorption in Multidirectional Waves.* IAHR seminar on Multidirectional Waves and their Interaction with Structures, 27th IAHR Congress, San Francisco, 10-15 August 1997.

Hydraulics and Coastal Engineering Laboratory (1997). *PADIWA - A Package for Directional Wave Analysis.* Hydraulics and Coastal Engineering Laboratory, Department of Civil Engineering, Aalborg University, January 1997.

NtH. *Bølger på dypt og grunt vann.* Institutt for Havnebyggning, Univeritetet i Trondheim, Norges tekniske Hogskole.

Allsop N. W. H., Vicinanza D. and McKenna J. E. (1996). *Wave Forces on Vertical and Composite Breakwaters.* Report SR 443, March 1995, revised 1996, HR Wallingford.

Franco, C., Franco, L., Restano, C., van der Meer, J.W. (1995). *The effect of wave obliquity and short-crestedness on the overtopping rate and volume distribution on caisson breakwaters.* Final proceedings, MAST II, (MAS2-CT92-0047), MCS-Project: Monolithic (Vertical) Coastal Structures, Paper 4.9.

9 Appendix A

9.1 Organisation of stored data and analysis results

The data from each performed test series has been stored on a seperate CD-R. Each test series is identified through a unique number used in file- and directory names with the following format:

vv_xx_yz.*

where

   vv denotes the target angle of wave attack θ.

xx is a number corresponding to the directional spreading σ. The number 15 corresponds to $\sigma = 25°$ and the number 25 corresponds to $\sigma = 18°$.

y is a counting number. $y = 1$ or 2 corresponds to two series with a configuration where pressures were sampled in section E, F, G and I, and a width of the overtopping measuring device of 0.3 m. $y = 3$ corresponds to a series with a configuration where the pressures were sampled in section A, C, G and J, and a width of the overtopping measuring device of 0.1 m.

z denotes the section. If $z = 1$ or 2 then 1, 2, 3 and 4 corresponds to section E, F, G and I, respectively. If $z = 3$ then 1, 2, 3 and 4 corresponds to section A, C, G and J, respectively. y = 0 is used for the samples of the measured elevations.

The extensions in the filenames of the files stored on the CD-R's denotes the contents of the files. In Table 3 a list of the used extensions are shown with a discription of the corresponding filetype.

Extension	Description
BIN	Measured pressures sampled as binary reals an stored as words (2 bytes).
PRE	Measured pressures in ASCII format obtained by converting the PRE files by use of the program BINTOASC.exe found in the PROGRAMS directory.
FOR	Time (column 1), horizontal force (column 2) and distance from bottum of caisson to the resulting horizontal force (column 3) obtained by analyzing the BIN-files by use of the program HORIFORC.exe found in the PROGRAMS directory.
CAL	Calibration constants.
ETA	Sampled elevations from the 7 wave gauges used in the 3D analysis of the wave field (column 1 - 7), the 4 wave gauges used to measure the waves at the sections (column 8 - 11) and the water level in the overtopping measuring device (column 12).
ZUP	Setup file for use of the 3D wave analysis program found in the PROGRAMS\BDM directory.
SPC	File used by the 3D wave analysis program found in the PROGRAMS\BDM directory.
BDM	File used by the 3D wave analysis program found in the PROGRAMS\BDM directory.
RES	Result file from the 3D wave analysis program found in the PROGRAMS\BDM directory.

Table 3: Description of file extensions for the files found on the CD-R's with test data.

Furthermore, the input files for use with the active wave absorption system have been save in a seperate directory on some of the CD-R's labeled OSW, which is also used as the extension on the files.

All the text files, drawings, spreadsheet and other files files (AutoCAD, LaTeX, DataPlot, Word, Excel etc.) used in the analysis and description of the performed tests are stored on the CD-R labeled ANALYSIS.
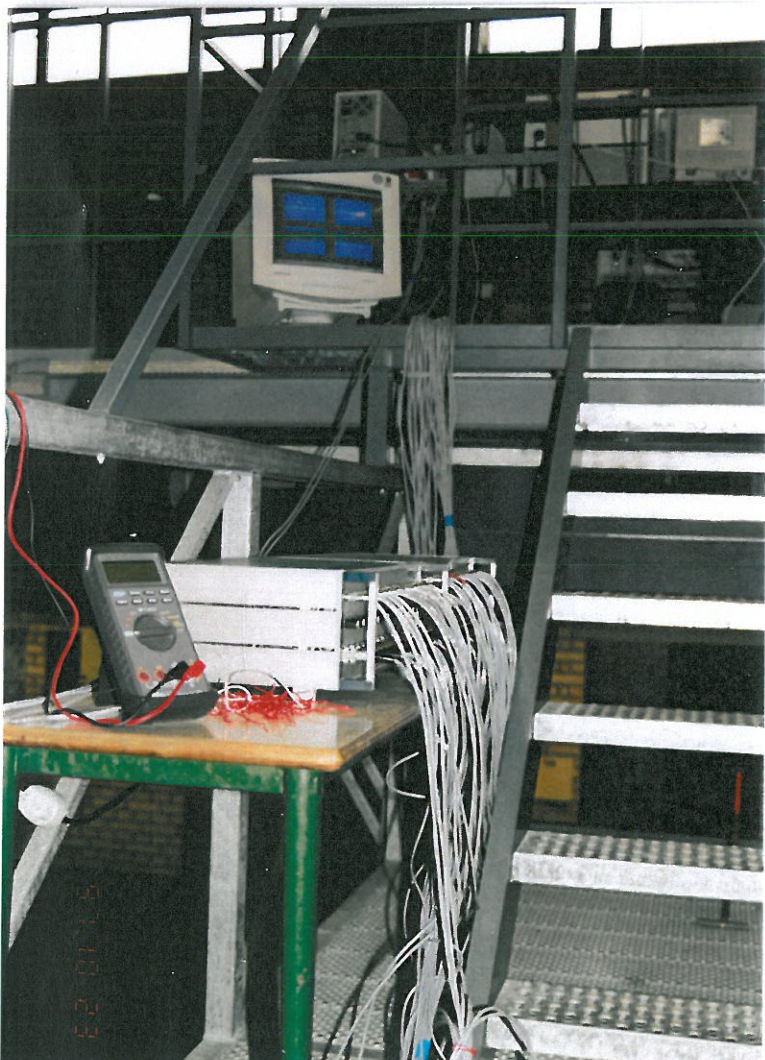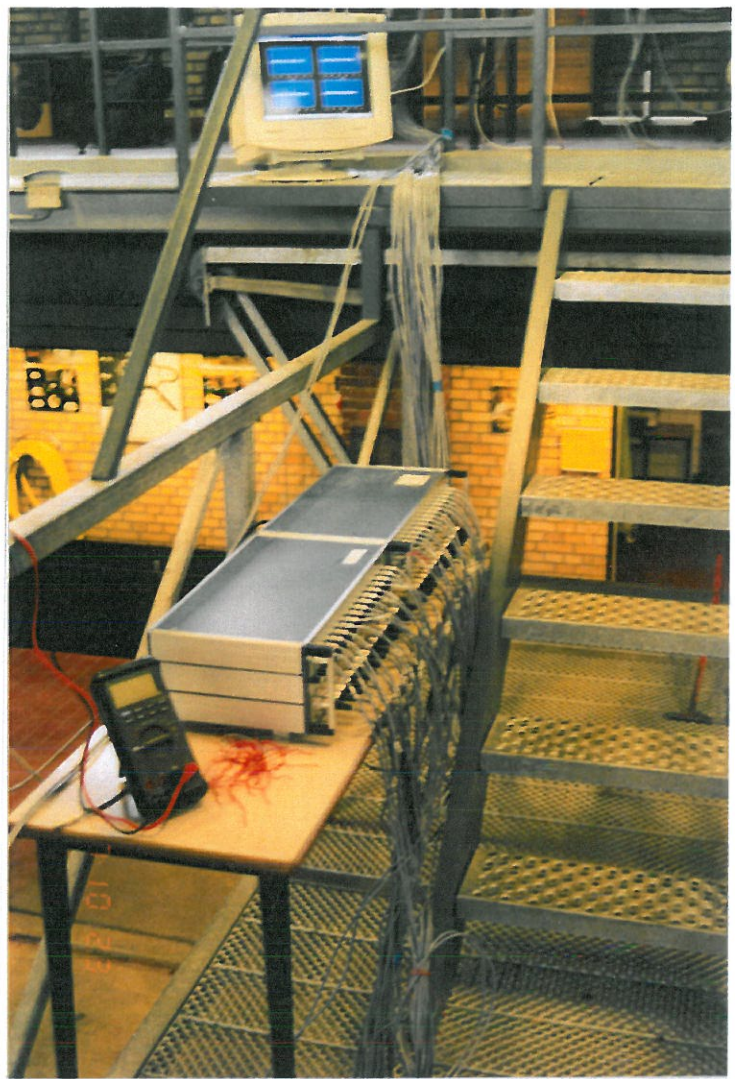
10 Appendix B

10.1 Photos

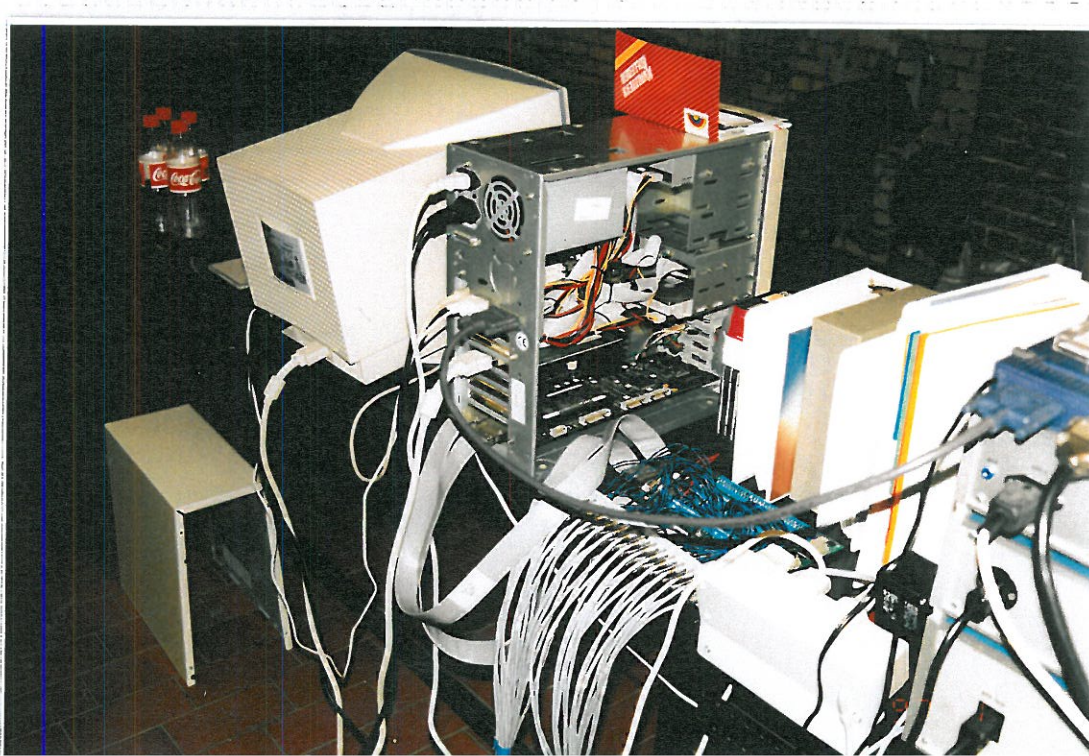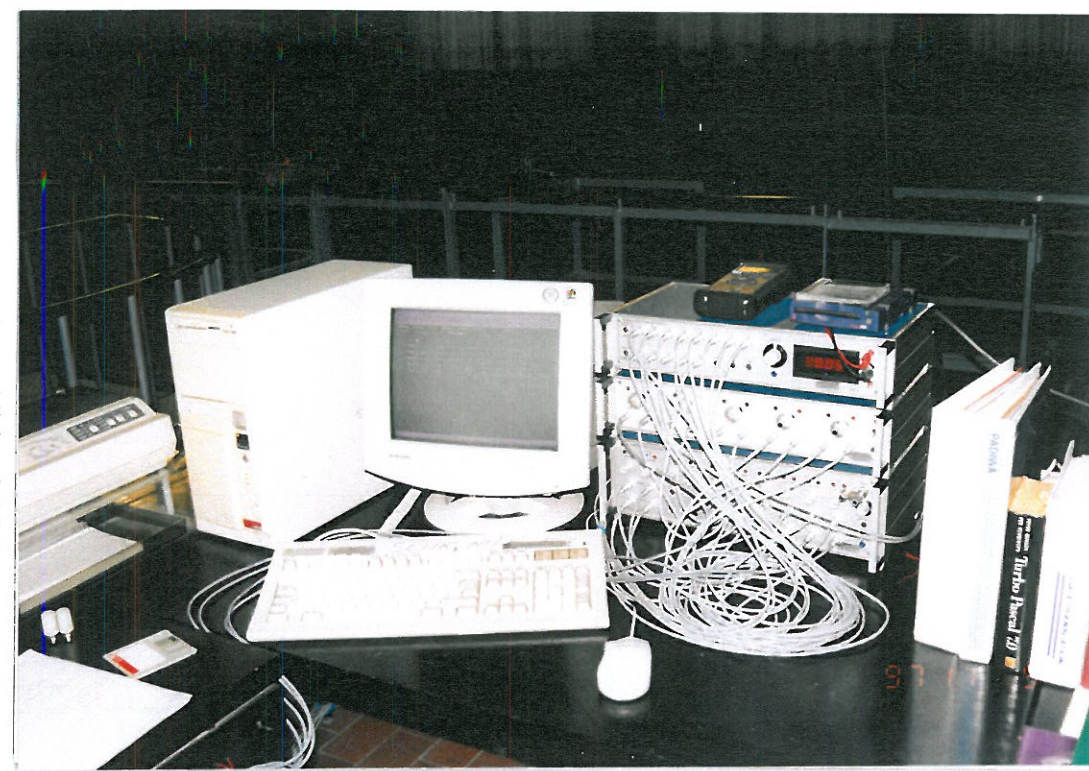On the following pages pictures taken through out work in the laboratory.

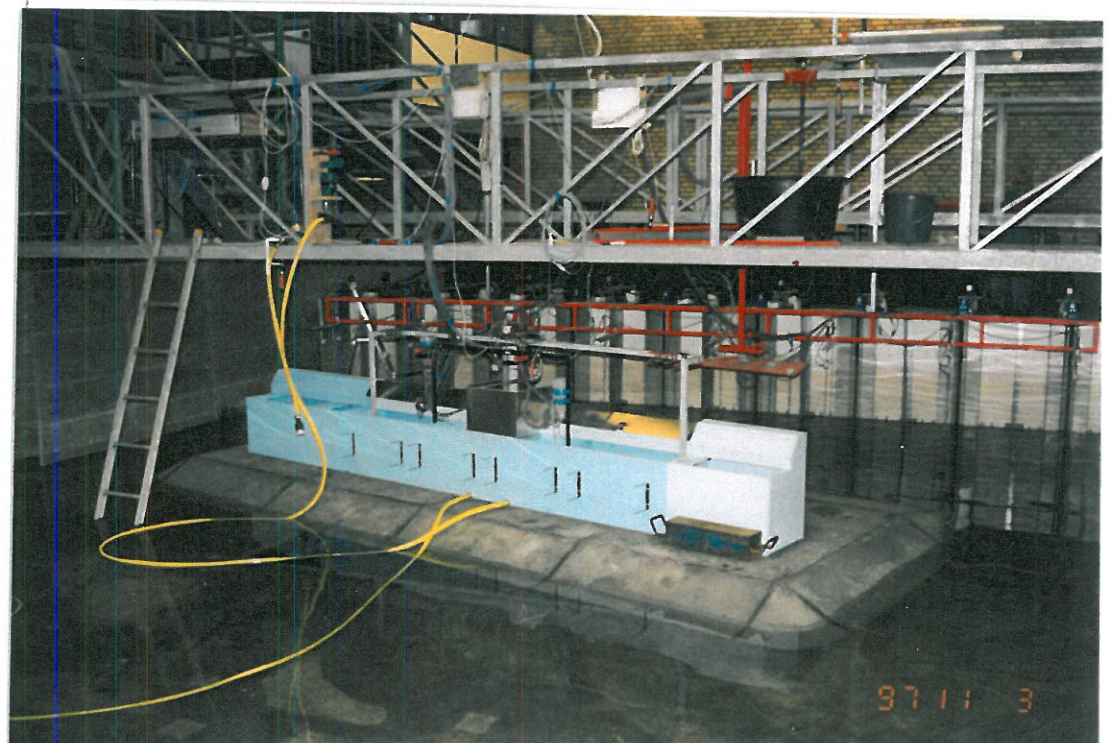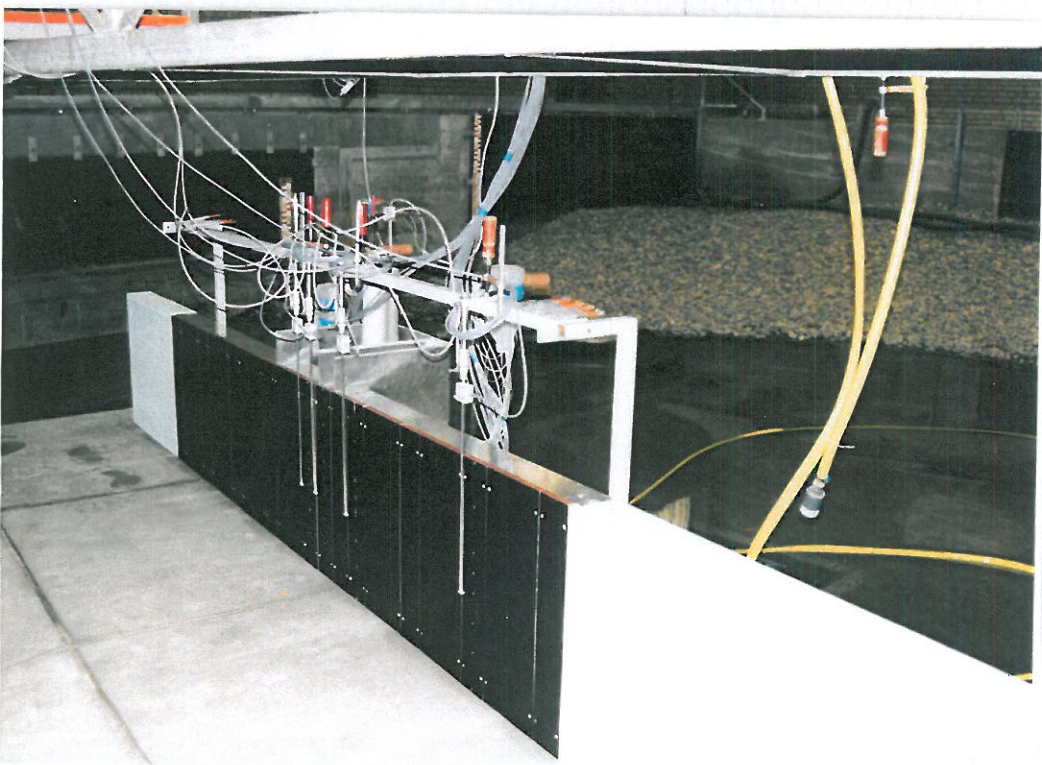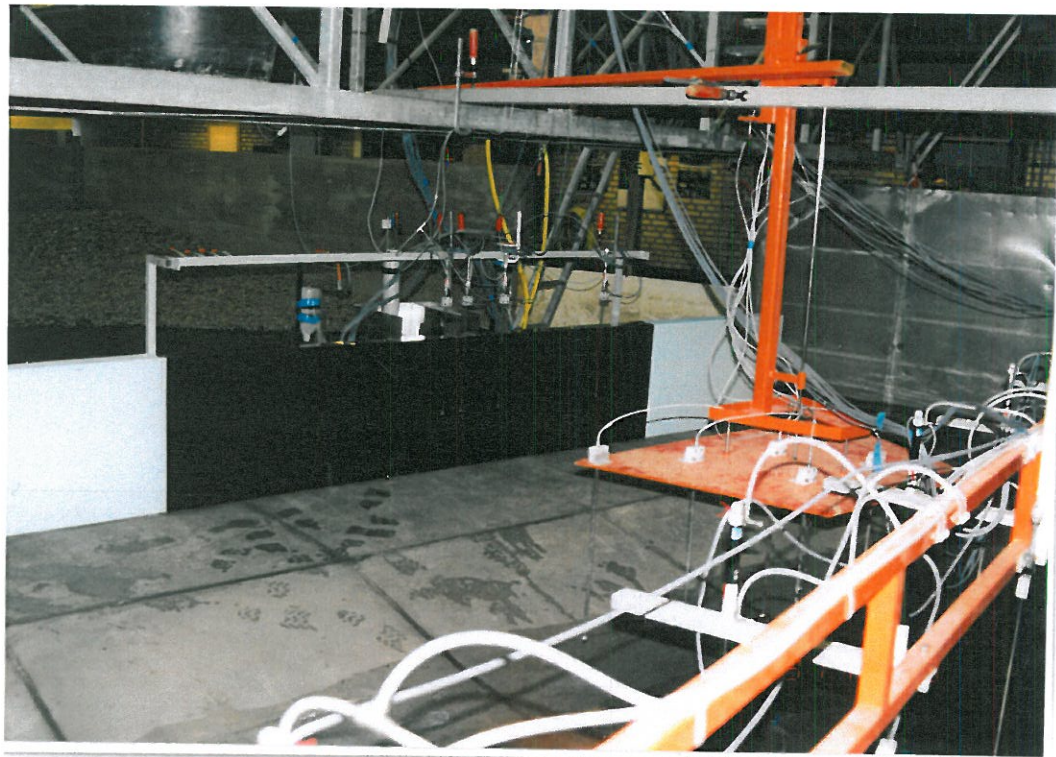Equipment used for sampling the data from the measuring devices and storing it on computers

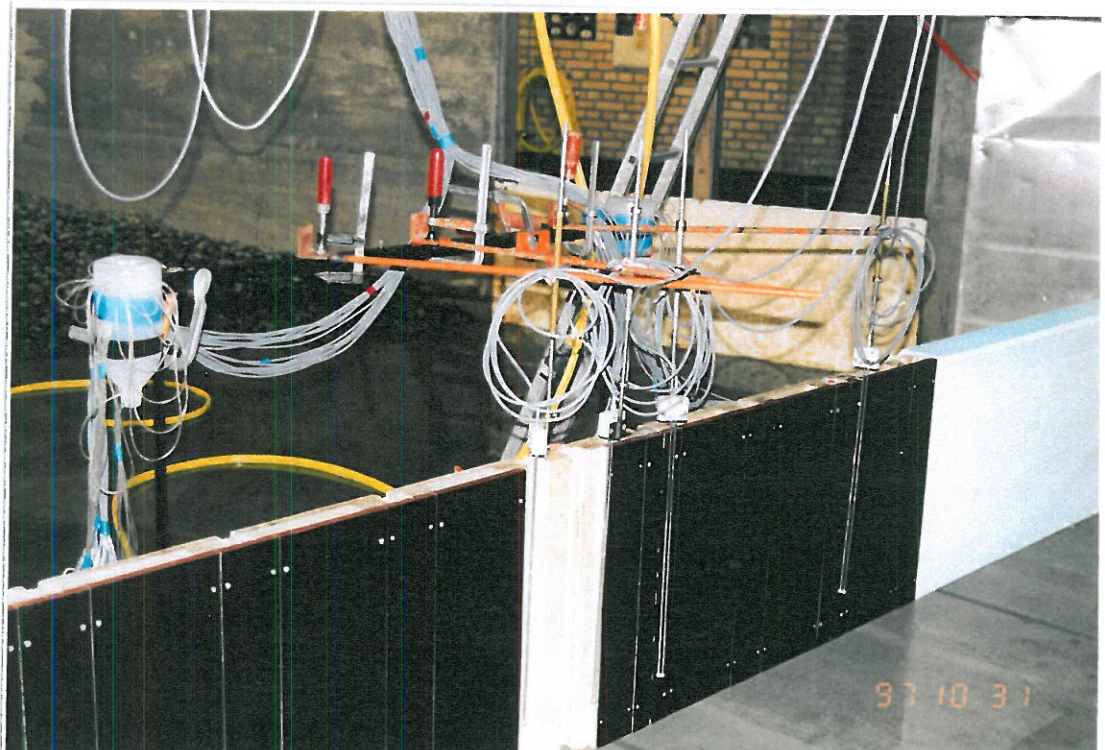The model structure and the layout of the wave tank.

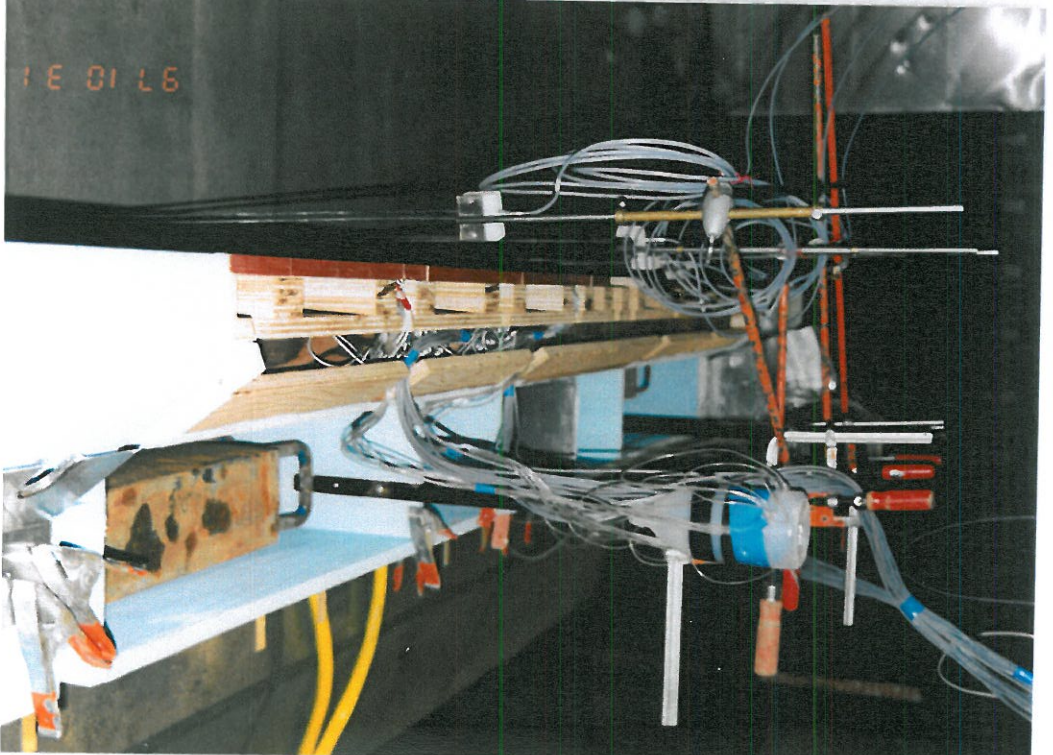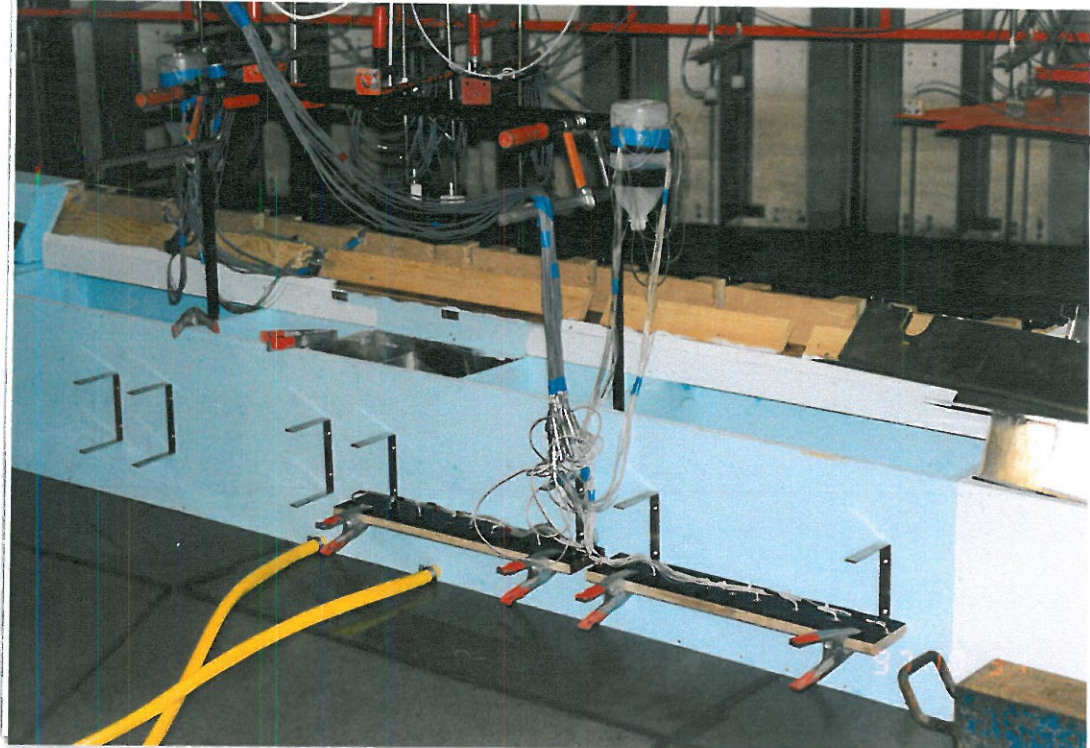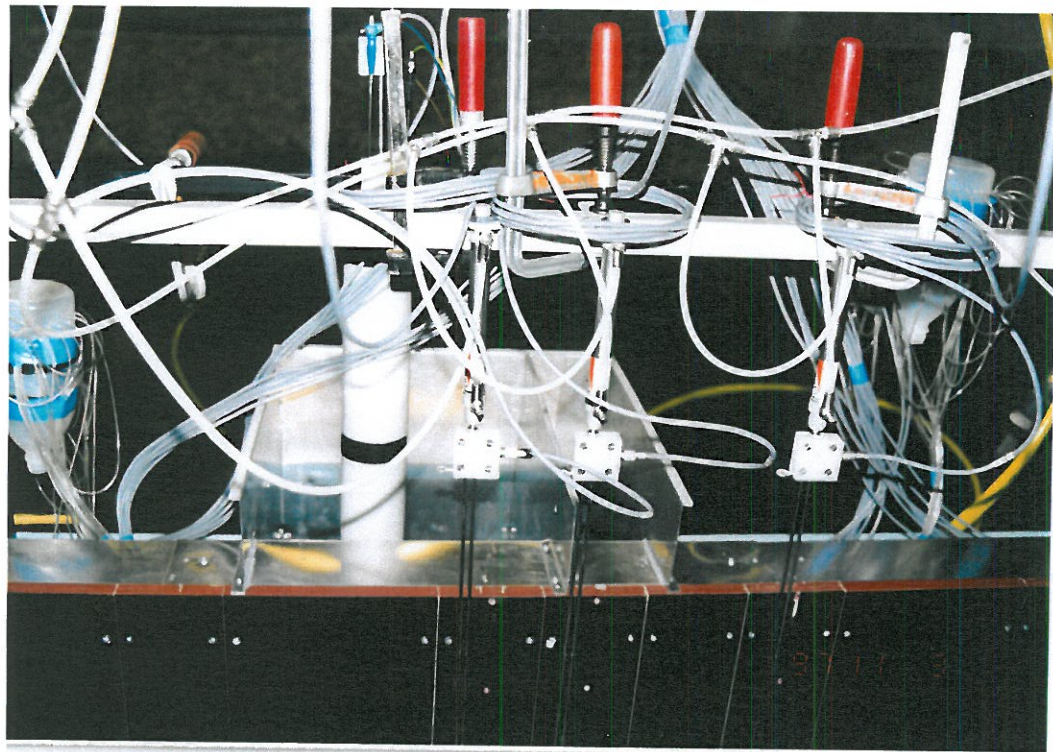The setup of the structure and the measuring devices in the wave tank.

The structure in the different performed tests.